A&A 411, 587–593 (2003)
DOI: 10.1051/0004-6361:20031398

Astronomy & Astrophysics

AD Leonis: Flares observed by XMM-Newton and Chandra

E. J. M. van den Besselaar[1,2], A. J. J. Raassen[1,3], R. Mewe[1], R. L. J. van der Meer[1], M. Güdel[4], and M. Audard[5]

[1] SRON National Institute for Space Research, Sorbonnelaan 2, 3584 CA Utrecht, The Netherlands
e-mail: A.J.J.Raassen@sron.nl;R.Mewe@sron.nl;R.L.J.van.der.Meer@sron.nl
[2] Department of Astrophysics, University of Nijmegen, PO Box 9010, 6500 GL Nijmegen, The Netherlands
[3] Astronomical Institute "Anton Pannekoek", Kruislaan 403, 1098 SJ Amsterdam, The Netherlands
[4] Paul Scherrer Institut, Würenlingen & Villigen, 5232 Villigen PSI, Switzerland
e-mail: guedel@astro.phys.ethz.ch
[5] Columbia Astrophysics Laboratory, Columbia University, 550 West 120th Street, New York, NY 10027, USA
e-mail: audard@astro.columbia.edu

Received 3 February 2003 / Accepted 2 September 2003

Abstract. The M-dwarf AD Leonis has been observed with the Reflection Grating Spectrometers and the European Photon Imaging Camera aboard XMM-Newton and also with the Low Energy Transmission Grating Spectrometer aboard the Chandra X-ray Observatory. In the observation taken with XMM-Newton five large flares produced by AD Leo were identified and only one in the observation taken with Chandra. A quiescent level to the lightcurves is difficult to define, since several smaller flares mutually overlap each other. However, we defined a quasi-steady state outside of obvious flares or flare decays. The spectra from the flare state and the quasi-steady state are analysed separately. From these spectra the temperature structure was derived with a multi-temperature model and with a differential emission measure model. The multi-temperature model was also used to determine the relative abundances of C, N, O, Ne, Mg, Si, S, and Fe. He-like ions, such as O VII and Ne IX, produce line triplets which are used to determine or constrain the electron temperature and electron density of the corresponding ion. During the flare state a higher emission measure at the hottest temperature is found for both XMM-Newton and Chandra observations. The derived abundances suggest the presence of an *inverse* First Ionization Potential effect in the corona of AD Leo.

Key words. stars: individual: AD Leonis – stars: coronae – stars: flare – X-rays: stars – missions: XMM-Newton, Chandra

1. Introduction

AD Leo is an M-dwarf with spectral type M3.5 V at a distance of 4.7 parsec[1]. Many cool stars (F–M) maintain active coronae with temperatures up to 20 MK. Our goal is to determine differences in the physical coronal conditions such as temperatures, emission measures, abundances, and densities between different states of the corona of AD Leo. We note that in the corona of the Sun a First Ionization Potential (FIP) effect is observed (Feldman 1992) which implies that elements with a low FIP (say $\lesssim$10 eV) are enhanced in the corona relative to the photospheric values. But for other active stars an *Inverse* FIP (IFIP) effect was suggested (Brinkman et al. 2001; Güdel et al. 2001). The underlying mechanism for these FIP and IFIP effects is not well understood. In this paper, the abundances are measured to see if there are anomalies and whether these are different for the flare state and quasi-steady state.

AD Leo is known to be capable of frequent flaring in the X/EUV/optical regime (Kahn et al. 1979; Pettersen et al. 1984; Pallavicini et al. 1989; Hawley et al. 1995; Cully et al. 1997). Flares on M-dwarfs may play a part in the heating mechanism of the outer atmospheres of stars. Audard et al. (2000), Kashyap et al. (2002), and Güdel et al. (2003) describe this mechanism. They suggest that the "quiescent" emission is in fact a superposition of multiple small flares. The expression "quasi-steady" is therefore used in this paper to refer to the state between the distinct flares.

Here we investigate the high-resolution spectra of AD Leo taken by the XMM-Newton satellite and the Chandra X-ray Observatory. The outline of this paper is the following. First, both observations are discussed. Section 3 gives the procedures followed to reduce the data. Section 4 describes the data analysis of the XMM-Newton observation during the flaring and quasi-steady states, whereas Sect. 5 describes the analysis for the Chandra observation. In Sect. 6 we discuss our results, and finally in Sect. 7 our conclusions are given.

2. Observations

On May 14, 2001 AD Leo was observed by XMM-Newton. Here we investigate the spectra taken with the two Reflection Grating Spectrometers, RGS, and the European Photon Imaging

Send offprint requests to: E. J. M. van den Besselaar,
e-mail: besselaar@astro.kun.nl

[1] SIMBAD Database: http://simbad.u-strasbg.fr/sim-fid.pl

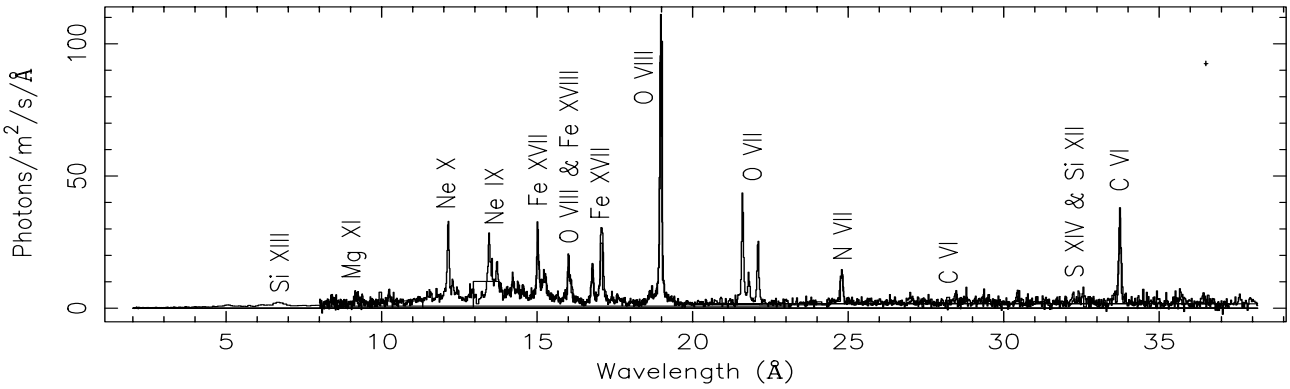

Fig. 1. The X-ray spectra taken by RGS 1, RGS 2 and EPIC-MOS 2 aboard XMM-Newton. The dominant lines in the spectrum have been labeled with the corresponding ion. EPIC-MOS 2 has a lower resolution and is used only from ∼2 to ∼14 Å. RGS 1 and 2 have a higher resolution and are used from 8 to 38 Å. A typical error bar for the continuum is included in the upper right corner.

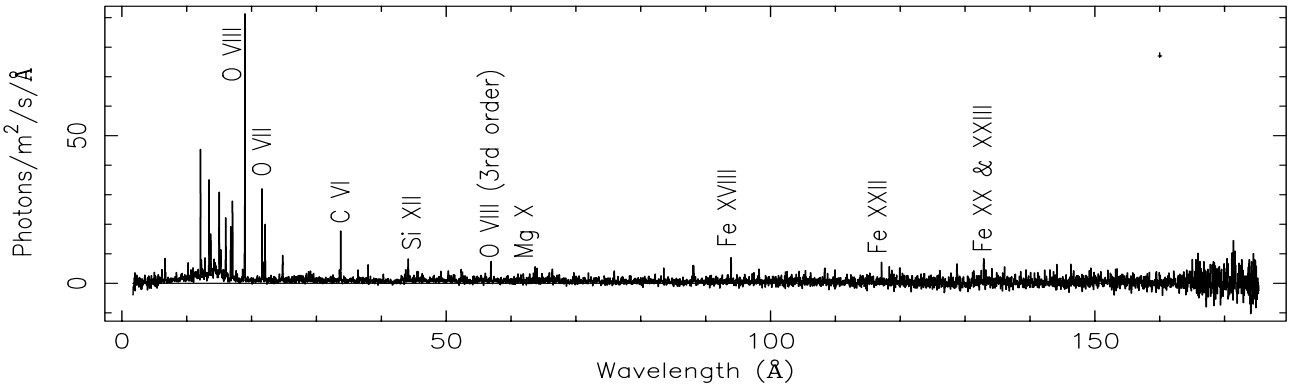

Fig. 2. The X-ray spectrum taken by LETGS aboard Chandra. The dominant lines in the spectrum have been labeled with the corresponding ion. The labels for lines below 20 Å can be found in Fig. 1. A typical error bar for the continuum is included in the upper right corner.

Table 1. The state of the instruments aboard XMM-Newton together with the corresponding observation times in seconds.

Instr.	Mode	Filter	Obs. Time
EPIC-MOS 2	large window	thick	35 824
RGS 1	spectro + q	not applicable	36 354
RGS 2	spectro + q	not applicable	36 354

Camera, EPIC-MOS 2. (EPIC-MOS 1 was in timing mode, EPIC-PN has less spectral resolution than the EPIC-MOS.) The spectral resolution of EPIC-MOS 2 is lower than that of RGS, but its sensitivity is higher. The exposure time was about 36 ks. The state of the instruments during this observation is given in Table 1 together with the total observation time of the corresponding instrument. In this observation no strong solar flares were detected and therefore no time intervals were rejected.

The spectrum of this dataset is shown in Fig. 1. The wavelength range used for RGS is 8 to 38 Å and the spectral line resolution is $\Delta\lambda \sim 0.07$ Å at full width at half maximum (FWHM). RGS has a wavelength accuracy of ∼8 mÅ and a maximum effective area of about 140 cm^2 around 15 Å (den Herder et al. 2001). The wavelength range used for EPIC-MOS 2 was constrained to ∼1.8 to ∼14 Å because of the better resolution of RGS at longer wavelengths. The background (about 1 photon m^{-2} s^{-1} Å^{-1}) has been subtracted from these spectra.

AD Leo was also observed, half a year earlier, with the Low Energy Transmission Grating Spectrometer (LETGS) aboard Chandra. This instrument has taken the X-ray spectrum on October 24, 2000 during an exposure time of 48.41 ks. The background-subtracted spectrum is shown in Fig. 2. The background consists of about 1 photon m^{-2} s^{-1} Å^{-1} below 60 Å and steadily increasing to about 8 photons m^{-2} s^{-1} Å^{-1} at ∼170 Å.

The LETGS consists of an imaging camera (HRC-S) with a grating spectrometer (LETG). At FWHM, this instrument has a spectral resolution of $\Delta\lambda \sim 0.06$ Å (Brinkman et al. 2000) and a wavelength uncertainty of a few mÅ below 30 Å, increasing to about 0.02 Å above. The wavelength range is 1 to 175 Å.

The number of photons m^{-2} s^{-1} Å^{-1} for the lines in the XMM-Newton spectra show a small difference from those of the Chandra spectra. We believe that the difference is due to different activity levels between the XMM-Newton and Chandra observations.

3. Data reduction

The spectra taken with the XMM-Newton satellite are pipelined using the XMM-Newton SAS, "Science Analysis System", version 5.3.3. This program reads the current calibration files of the instruments and the observation data files. The relevant information in these files is written to new files which contain the source spectrum, the background spectrum, and the

Table 2. Time intervals of the flares in seconds after the start of the XMM-Newton observation (t_0 = 52 043.8667 MJD).

No.	Begin	End
1	0	6400
2	13 400	18 400
3	25 400	27 400
4	28 900	30 700
5	33 400	35 400
Total flare state:		17.2 ks
Total quasi-steady state:		18.8 ks

response matrix with information about e.g., the line-spread-function and the effective area of each instrument used. To construct the RGS spectrum 95% of the cross-dispersion function of the data is used. In our analysis we have used only the first order spectrum.

To extract the spectrum of the EPIC-MOS 2 data a circle with a radius of 40″ around the image of AD Leo is taken. The response matrix and ancillary files, containing the effective area, are generated with SAS. To determine the background level, a circle with identical radius is used in a part of the detector without any sources.

The Chandra data is pipelined using the CIAO 2.2 program (Chandra Interactive Analysis of Observations). The spectrum, response matrix, and effective area files are determined by a local extracting software, using a bow-tie shaped region around the dispersion axis as extraction region for the spectrum. In our analysis of this observation we have co-added the +1 order and −1 order spectra. The background level is determined from a rectangular box 10″ − 40″ above and below the dispersion axis on the detector, to get the best statistics on the background. The background spectrum is then scaled per bin from the rectangular box to the size of the bow-tie in the corresponding wavelength bin.

We use the software package SPEX (Kaastra et al. 1996b) in combination with the updated MEKAL code (Mewe et al. 1995) for an optically thin plasma in Collisional Ionization Equilibrium (CIE)[2] to analyse the X-ray spectra of XMM-Newton and Chandra.

4. Data analysis of the XMM-Newton observation

In the lightcurve of the X-ray observation of AD Leo taken with EPIC-MOS 2 five flares are distinguished. The time intervals of the flares are given in Table 2 and shown in Fig. 3. We have analysed the summed time intervals of the flares (17.2 ks). Indeed, the signal-to-noise ratio of individual flares is too low to obtain clear results. It is difficult to clearly distinguish quiescent emission (if that exists) from the overlapping flare events. It is possible that no physical quiescent emission is present at all in the corona of AD Leo, but that the emission is produced by a superposition of multiple small flares (Audard et al. 2000; Kashyap et al. 2002; Güdel et al. 2003).

[2] http://www.sron.nl/divisions/hea/spex/version1.10/line/

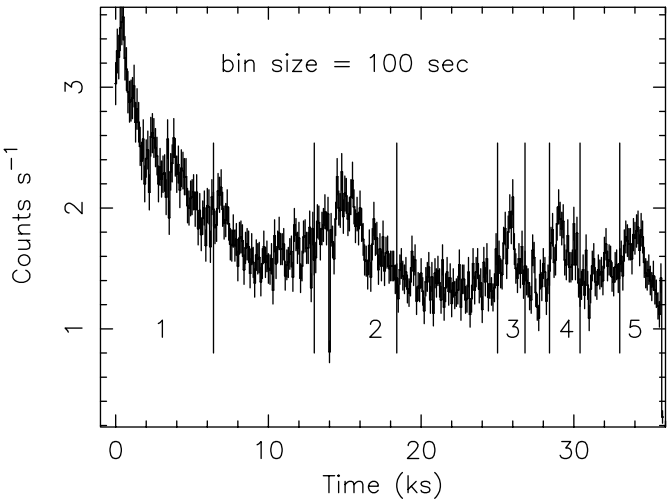

Fig. 3. Lightcurve of the observation taken by EPIC-MOS 2.

The temperature structure in the corona is determined in two different ways. First, we have measured the temperatures with a multi-temperature model using the MEKAL code. This model is simultaneously fitted to the RGS 1, RGS 2, and EPIC-MOS 2 spectra. The temperatures, emission measures, and abundances of several elements were derived from this model. The second method to determine the temperature structure is by use of a differential emission measure (DEM) model based on the polynomial method (Kaastra et al. 1996a). The used interstellar hydrogen column density ($N_{\rm H}$) is 3×10^{18} cm^{-2} (Cully et al. 1997).

4.1. Temperatures and abundances

A multi-temperature fit to the data was performed. From this model three temperatures and their corresponding emission measures were determined, together with the abundances of C, N, O, Ne, Mg, Si, S, and Fe. The χ^2 statistics did not improve when additional components were added. The results from this analysis are given in Table 3.

The uncertainties in this table are 1σ statistical uncertainties only. However we caution that additional systematic uncertainties exist. For example, a typical 10% uncertainty is present in the atomic database used to model the lines. Therefore abundances and EMs are affected by this uncertainty as well. Typically their total uncertainties will range from 15 to 20%.

Unfortunately, the continuum is not well constrained and the absolute abundances (relative to H) are thus not uniquely derived. Indeed, if the continuum level is difficult to measure, the EMs cannot be easily constrained. Incidentally any line flux can be modeled with any product of the elemental abundance and the EM, e.g., O/H$\cdot EM_{\rm total} \cong$ constant. On the other hand, an abundance ratio (e.g., relative to O) is rather stable and allow us to compare between the XMM-Newton and Chandra observations.

The abundances are relative to their corresponding solar photospheric values from Anders & Grevesse (1989), except for O, C, and Fe for which more recent values were used (Allende Prieto et al. 2001, 2002; Grevesse & Sauval 1999).

Table 3. Temperatures, emission measures, and coronal abundances of several elements as determined from the spectrum during the flares and quasi-steady state. The abundance ratios are relative to solar photospheric abundances (Col. 6; $\log A_{\rm H} = 12$). The numbers in parentheses are the statistical 1σ uncertainties. The X-ray luminosity ($L_{\rm X}$) is measured between 0.3 and 10 keV. $EM_{\rm total}$ is the total of the three given emission measures. Columns 2 and 3 give the results of the XMM-Newton observation, discussed in Sect. 4.1, and Cols. 4 and 5 those of the Chandra observation which are discussed in Sect. 5.1.

	XMM-Newton				Chandra				Solar Photospheric	
Parameter	Flare		Quasi-steady		Flare		Quasi-steady		Abundance	
T_1 (MK)	2.88	(0.06)	2.84	(0.06)	2.7	(0.1)	2.8	(0.1)		
EM_1 (10^{51} cm^{-3})	1.2	(0.1)	1.2	(0.1)	0.8	(0.1)	0.54	(0.07)		
T_2 (MK)	7.1	(0.1)	7.1	(0.1)	7.1	(0.3)	6.7	(0.2)		
EM_2 (10^{51} cm^{-3})	2.0	(0.2)	1.5	(0.1)	1.2	(0.2)	1.0	(0.1)		
T_3 (MK)	20.2	(1.0)	20.1	(1.5)	17.6	(1.5)	14.8	(1.9)		
EM_3 (10^{51} cm^{-3})	0.92	(0.07)	0.46	(0.05)	1.3	(0.1)	0.37	(0.06)		
$L_{\rm X}$ (10^{28} erg/s)	4.6		3.5		4.4		2.3			
Abun. C/O	1.6	(0.2)	1.7	(0.2)	1.7	(0.5)	1.8	(0.3)	$\log A_{\rm C}$	8.39
Abun. N/O	1.0	(0.1)	0.9	(0.1)	1.1	(0.3)	0.8	(0.2)	$\log A_{\rm N}$	8.05
Abun. O/O	1.00	(0.09)	1.0	(0.1)	1.0	(0.2)	1.0	(0.1)	$\log A_{\rm O}$	8.69
Abun. Ne/O	1.1	(0.1)	1.2	(0.1)	1.4	(0.3)	1.2	(0.2)	$\log A_{\rm Ne}$	8.09
Abun. Mg/O	0.48	(0.07)	0.54	(0.09)	0.5	(0.2)	0.21	(0.08)	$\log A_{\rm Mg}$	7.58
Abun. Si/O	0.8	(0.1)	0.9	(0.1)	0.8	(0.2)	1.0	(0.1)	$\log A_{\rm Si}$	7.55
Abun. S/O	0.6	(0.1)	0.6	(0.1)	0.3	(0.1)	0.3	(0.1)	$\log A_{\rm S}$	7.21
Abun. Fe/O	0.46	(0.05)	0.48	(0.05)	0.44	(0.09)	0.35	(0.04)	$\log A_{\rm Fe}$	7.50
Abun. O/H	0.74	(0.05)	0.71	(0.05)	1.0	(0.1)	1.1	(0.1)		
O/H·$EM_{\rm total}$	3.1	(0.3)	2.2	(0.2)	3.3	(0.4)	2.1	(0.2)		
χ^2/d.o.f.	5598/4574		5529/4574		1700/1428		5271/4532			

To study differences between the flare state and quasi-steady state, the latter has been analysed as well. The results from this analysis are also given in Table 3. The emission measure of the two highest temperatures is significantly lower for the quasi-steady state than for the flare state. The abundances, however, do not show a significant difference between the flares and the quasi-steady state.

4.2. DEM modeling

To determine a smoother temperature distribution a DEM modeling is performed for the two data sets consisting of the flare state and quasi-steady state. Kaastra et al. (1996a) describe different methods to determine the differential emission measure distribution which are based on a clean, polynomial, or regularization method. The polynomial method with order eight is used here to derive the emission measure distribution of these spectra, but the results of the other methods are in agreement. The abundances derived from fitting them simultaneously with the emission measure distribution agree very well with those received from the multi-temperature fit. The derived distribution is shown in Fig. 4 for both states. During the flare state the emission measure of the highest temperature range is higher.

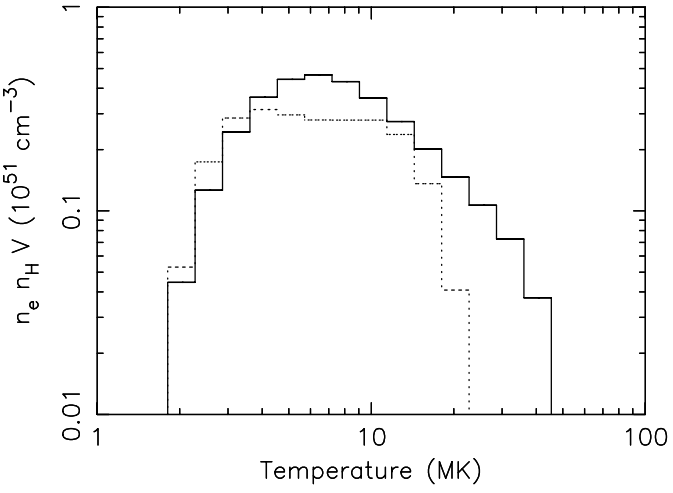

Fig. 4. The differential emission measure, as obtained from the polynomial method with order eight, during the flare state (solid line) and quasi-steady state (dotted line) of AD Leo as measured with XMM-Newton.

4.3. Analysis of He-like ions

The helium-like ions, such as O VII and Ne IX, produce the well-known line triplets in the spectrum. Such a triplet consists of a resonance (r), forbidden (f), and an intercombination (i) line. The flux ratios of these lines are dependent on the electron temperatures and densities. A higher density results in weaker forbidden lines and stronger intercombination lines. Therefore the line flux ratio f/i is a density sensitive quantity.

The O VII line triplet is located between 21.6 and 22.1 Å. The fluxes of these lines have been measured during both states of AD Leo. The values are given in Table 4. In the

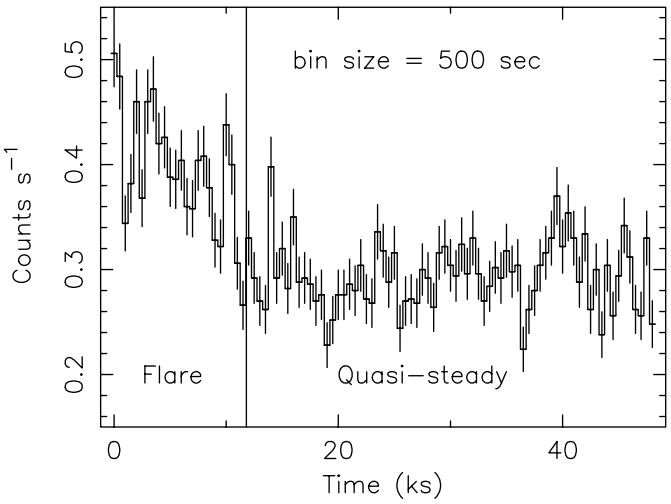

Fig. 5. The zeroth order lightcurve of the observation taken by LETGS.

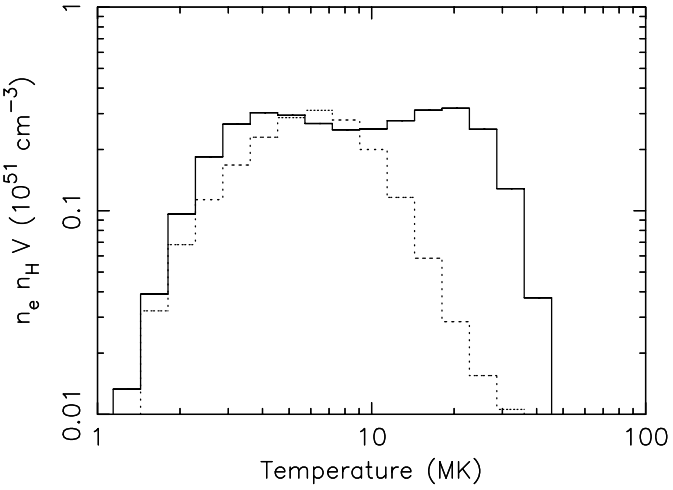

Fig. 6. The differential emission measure, as obtained from the polynomial method with order eight, during the flare state (solid line) and quasi-steady state (dotted line) of AD Leo as measured with Chandra.

multi-temperature model the abundance of O is set to zero and the other abundances, temperatures, and emission measures are fixed at the values given in Table 3. The effect to the continuum by setting the abundance of O to zero is negligible. Three delta functions are added on top of this model to measure the contribution of O to these lines in a small wavelength range around the O lines. These delta functions are convolved with the instrumental line profile and their amplitudes are fitted to the observations. With this procedure we have corrected for possible blends by other lines at these wavelengths and only the contribution of O is measured. For the Ne IX line triplet the same procedure is applied. The effect to the continuum by setting Ne to zero is negligible as well. Due to detector failure the O VII lines could only be measured in the spectrum taken with RGS 1 and the Ne IX lines in the spectrum of RGS 2 only. The fluxes for the Ne IX lines are also given in Table 4. The densities derived from Ne IX are less reliable due to blending by several Fe lines.

With the use of two flux ratios ($G = (f + i)/r$ and $R = f/i$) in combination with the tables of Porquet et al. (2001), the electron temperatures and densities are derived for the corresponding ions. The results are presented in Table 5. The electron temperature and upper limits of the electron density for O VII are higher during the flare state as compared to the quasi-steady state, but the difference is not formally significant. These temperatures and densities are representative for those plasmas in which the He-like lines are formed, and form only part of the range presented in Fig. 4.

5. Data analysis of the Chandra observation

The lightcurve from the LETGS spectrum is produced by taking the counts in a small circle around the zeroth order image of AD Leo with a radius of 1.4″. From this lightcurve, Fig. 5, we conclude that one flare was produced by AD Leo at the beginning of the observation (t_0 = 51 841.6286 MJD). This flare lasted for 11.8 ks. The remainder of the dataset (37.5 ks) is used to describe the quasi-steady state. As mentioned before, we cannot clearly speak of quiescent emission.

Just like for the XMM-Newton spectra, a multi-temperature fit and a DEM model were performed for the data to derive the temperature structure.

5.1. Temperatures and abundances

A multi-temperature fit is performed to the data based on CIE plasmas. From this model three temperatures were derived together with the corresponding emission measures. These results and the derived abundances are given in Table 3 together with the values for the XMM-Newton observation. For the same reason as in Sect. 4.1 the abundances are normalized to O.

5.2. DEM modeling

From the flare spectrum and quasi-steady spectrum a differential emission measure distribution is derived as shown in Fig. 6. This emission measure distribution is produced by the polynomial method with order eight. From this figure we conclude that the high temperature range has a larger contribution to the flare spectrum compared with the quasi-steady state. The other temperatures have roughly the same contribution. Also in this case, the results from the other methods agree very well with the DEM distribution and abundances already given in this paper.

5.3. Analysis of He-like line triplets

In the spectrum taken with Chandra, the line triplets produced by He-like ions are present as well. We have measured the fluxes of the O VII and Ne IX lines in the same way as the triplets in the XMM-Newton spectra. The fluxes for both the flare and quasi-steady state are given in Table 4 together with the fluxes as measured from the XMM-Newton observation. In this spectrum also the line triplet produced by Si XIII between 6.6 and 6.8 Å is present, but the fluxes of these lines are not significant enough to obtain a constraint on the electron temperature and density.

Table 4. Fluxes in ph s^{-1} m^{-2} measured at Earth for some He-like lines as determined from RGS 1 (O VII) and 2 (Ne IX) are given in Cols. 3 and 4, while the fluxes from the LETGS are given in Cols. 5 and 6. (See Sects. 4.3 and 5.3 for more information.)

		XMM-Newton		Chandra	
Ion	λ(Å)	Flare	Quasi-steady	Flare	Quasi-steady
O VII (r)	21.59	3.7 (0.4)	3.7 (0.4)	3.6 (0.7)	3.3 (0.4)
O VII (i)	21.80	1.0 (0.2)	0.8 (0.3)	1.3 (0.5)	0.7 (0.2)
O VII (f)	22.09	1.7 (0.3)	2.2 (0.2)	3.1 (0.6)	2.0 (0.3)
Ne IX (r)	13.44	2.6 (0.3)	1.7 (0.3)	2.1 (0.4)	1.9 (0.2)
Ne IX (i)	13.53	0.4 (0.3)	0.4 (0.3)	0.4 (0.3)	0.5 (0.2)
Ne IX (f)	13.69	1.5 (0.3)	1.1 (0.2)	1.5 (0.4)	1.2 (0.2)

Table 5. The electron temperatures T_e (MK) and electron densities n_e (cm $^{-3}$) as derived from the tables of Porquet et al. (2001) for the XMM-Newton observation (Cols. 2 and 3, Sect. 4.3) and for the Chandra observation (Cols. 4 and 5, Sect. 5.3). The numbers in parentheses are the 1σ uncertainties, and the upper and lower limits are 1σ limits.

	XMM-Newton		Chandra	
Ion	T_e (flare)	T_e (quasi-steady)	T_e (flare)	T_e (quasi-steady)
O VII	3 (1)	2.5 (1.0)	<2.5	2.5 (1)
Ne IX	4 (2)	3.0 (1.2)	<6.5	<5

Ion	n_e (flare)	n_e (quasi-steady)	n_e (flare)	n_e (quasi-steady)
O VII	$3\times10^{10} < n_e < 1\times10^{11}$	$<3\times10^{10}$	$1\times10^{9} < n_e < 7\times10^{10}$	$<3\times10^{10}$
Ne IX	$<3\times10^{12}$	$<3.5\times10^{12}$	$<3.5\times10^{12}$	$<7\times10^{11}$

From the fluxes of these He-like triplets the electron temperatures and electron densities of the respective ions were derived using the tables of Porquet et al. (2001). The obtained temperatures and densities are given in Table 5. These temperatures and densities are representative for those plasmas in which the He-like lines are formed, and form only part of the range presented in Fig. 6.

6. Discussion

6.1. Flaring versus quasi-steady state

The flare state and quasi-steady corona of the M-dwarf AD Leo have been analysed in both the XMM-Newton and Chandra spectra. Therefore the results are compared to determine the conditions during a flare and the state between the flares. As mentioned before, the quasi-steady emission is not clearly the quiescent emission, if such exists, but can possibly be identified with a superposition of decaying flares, and additional smaller flares.

From the DEM model, a difference between the flare and quasi-steady state can be seen for both observations. The relatively low (~3 MK) and intermediate (~7 MK) temperature ranges are present in almost the same amounts in both states. The difference appears in the emission measure of the highest temperature range (20−30 MK). The contribution of these temperatures is higher during the flare state. This is just as expected for a large flare. Smaller flares get less hot, and therefore the emission measure of the high temperature range is smaller during the quasi-steady state. Also the electron temperatures derived from the He-like line triplets are slightly higher during a flare.

6.2. Abundances

The corona of the Sun, which is less active than the corona of AD Leo, shows a first ionization potential effect. As explained in Sect. 4.1 the absolute abundance measurements are very uncertain, and therefore relative abundances are given. There is no significant difference in the relative abundances of the different elements during the flare state and the quasi-steady state. Therefore the average coronal abundances are plotted in Fig. 7 against the first ionization potential (FIP) of the corresponding element for the XMM-Newton observations as well as for the Chandra observation. Elements with a low FIP (<10 eV) are somewhat depleted, instead of enhanced, with respect to the solar photospheric values.

Despite the difficulty to obtain reliable absolute abundances (because the continuum is poorly determined and thus the absolute level of the EM may be equally uncertain), relative abundances show a clear pattern which will allow us to compare that to the pattern of the Sun and other (active) stars. Our results may thus indicate the presence of a weak *inverse* FIP effect in the corona of AD Leo. The value of carbon is too high to fit into the overall picture of an inverse FIP effect. In our analysis the most recent value of the C abundance in the solar photosphere (Allende Prieto et al. 2002) is used. By using the C abundance of Anders & Grevesse (1989), our value of C/O would shift downwards by a factor of 1.5 and this abundance comes more in line with the other high FIP elements.

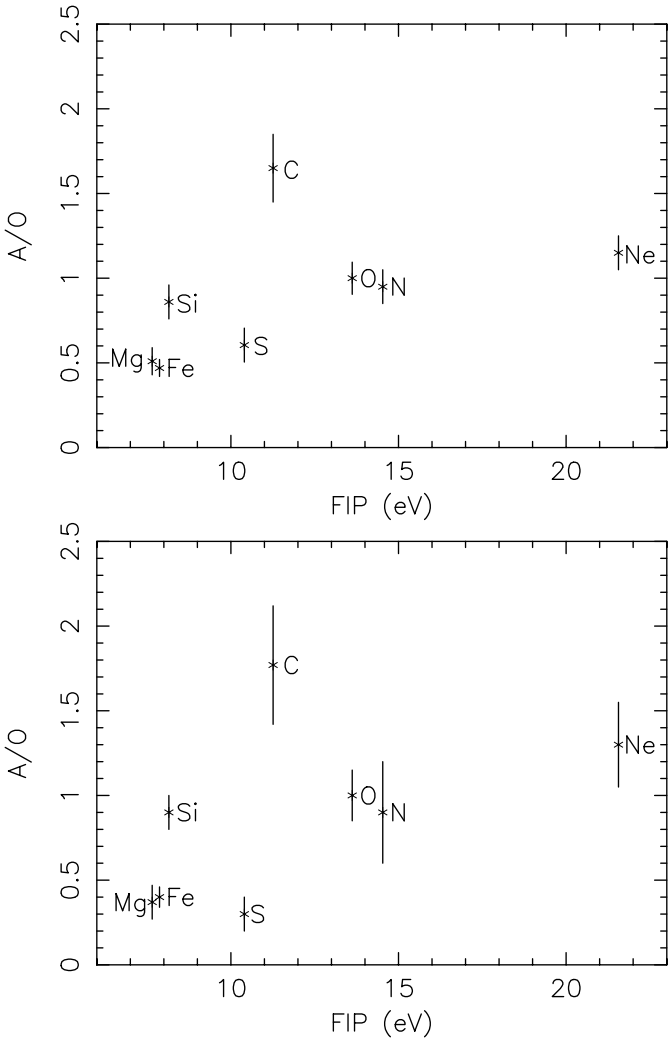

Fig. 7. Abundances versus the corresponding first ionization potentials as measured with XMM-Newton (top) and Chandra (bottom).

One possible effect for this high C abundance is that the *EM* at low temperatures is not well constrained by the XMM-Newton data. Therefore the C abundance, which is essentially formed at low temperatures, is less certain.

7. Conclusions

The physical properties of the corona of AD Leo are derived from observations of two different satellites, XMM-Newton and Chandra. The results from this analysis are in good agreement for both observations.

One can distinguish for the flare state a broad range in temperatures from about 1 to 40 MK, and for the quasi-steady state a range from 1 to 20 MK. The corresponding emission measures are not the same during these states. The flare state has a higher emission measure for the temperatures in the highest temperature range, which means that this temperature has a higher contribution to the flare spectra than to the spectra of the quasi-steady state.

From the line triplets of some He-like ions the electron temperatures and upper limits of the electron densities were derived, which are representative for those plasmas in which He-like ions are formed. These temperatures form only part of the range presented by the DEM models. The results from this analysis show higher electron temperatures during the flare state and also higher upper limits of most of the electron densities, but these higher upper limits may be due to different signal-to-noise ratios.

The abundances, however, do not show a significant difference between the flare state and the quasi-steady state. The derived average abundances from the total XMM-Newton observation as well as for the total Chandra observation are plotted against their first ionization potential. These figures suggest the presence of an *inverse* FIP effect in the corona of AD Leo. This is in contrast with the Sun, but in agreement with other active stars (HR 1099: Brinkman et al. 2001; AB Dor: Güdel et al. 2001).

Acknowledgements. The SRON National Institute for Space Research is supported financially by NWO. MG and MA acknowledge support from the Swiss National Science Foundation (grant 2000-058827 and fellowship 81EZ-67388, respectively).

Based on observations obtained with XMM-Newton, an ESA science mission with instruments and contributions directly funded by ESA Member States and the USA (NASA).

References

Allende Prieto, C., Lambert, D. L., & Asplund, M. 2001, ApJ, 556, L63
Allende Prieto, C., Lambert, D. L., & Asplund, M. 2002, ApJ, 573, L137
Anders, E., & Grevesse, N. 1989, Geochim. Cosmochim. Acta, 53, 197
Audard, M., Güdel, M., Drake, J. J., & Kashyap, V. L. 2000, ApJ, 541, 396
Brinkman, A. C., Behar, E., Güdel, M., et al. 2001, A&A, 365, L324
Brinkman, A. C., Gunsing, C. J. T., Kaastra, J. S., et al. 2000, ApJ, 530, L111
Cully, S. L., Fisher, G. H., Hawley, S. L., & Simon, T. 1997, ApJ, 491, 910
den Herder, J. W., Brinkman, A. C., Kahn, S. M., et al. 2001, A&A, 365, L7
Feldman, U. 1992, Phys. Scr., 46, 202
Grevesse, N., & Sauval, A. J. 1999, A&A, 347, 348
Güdel, M., Audard, M., Briggs, K., et al. 2001, A&A, 365, L336
Güdel, M., Audard, M., Kashyap, V. L., Drake, J. J., & Guinan, E. F. 2003, ApJ, 582, 423
Hawley, S. L., Fisher, G. H., Simon, T., et al. 1995, ApJ, 453, 464
Kaastra, J. S., Mewe, R., Liedahl, D. A., et al. 1996a, A&A, 314, 547
Kaastra, J. S., Mewe, R., & Nieuwenhuijzen, H. 1996b, in UV and X-ray Spectroscopy of Astrophysical and Laboratory Plasmas, ed. K. Yamashita, & T. Watanabe (Tokyo: Universal Academy Press, Inc.), 411 (SPEX)
Kahn, S. M., Linsky, J. L., Mason, K. O., et al. 1979, ApJ, 234, L107
Kashyap, V. L., Drake, J. J., Güdel, M., & Audard, M. 2002, ApJ, 580, 1118
Mewe, R., Kaastra, J. S., & Liedahl, D. A. 1995, Legacy, 6, 16 (MEKAL)
Pallavicini, R., Tagliaferri, G., & Stella, L. 1989, A&A, 228, 403
Pettersen, B. R., Coleman, L. A., & Evans, D. S. 1984, ApJS, 54, 375
Porquet, D., Mewe, R., Dubau, J., Raassen, A. J. J., & Kaastra, J. S. 2001, A&A, 376, 1113